



UNIVERSITY OF LEEDS

This is a repository copy of *Sea surface temperature control on the distribution of far-traveled Southern Ocean ice-rafted detritus during the Pliocene*.

White Rose Research Online URL for this paper:
<http://eprints.whiterose.ac.uk/80164/>

Version: Published Version

Article:

Cook, CP, Van De Flierdt, T, Hill, DJ et al. (8 more authors) (2014) Sea surface temperature control on the distribution of far-traveled Southern Ocean ice-rafted detritus during the Pliocene. *Paleoceanography*, 29 (6). 533 - 548. ISSN 0883-8305

<https://doi.org/10.1002/2014PA002625>

Reuse

Unless indicated otherwise, fulltext items are protected by copyright with all rights reserved. The copyright exception in section 29 of the Copyright, Designs and Patents Act 1988 allows the making of a single copy solely for the purpose of non-commercial research or private study within the limits of fair dealing. The publisher or other rights-holder may allow further reproduction and re-use of this version - refer to the White Rose Research Online record for this item. Where records identify the publisher as the copyright holder, users can verify any specific terms of use on the publisher's website.

Takedown

If you consider content in White Rose Research Online to be in breach of UK law, please notify us by emailing eprints@whiterose.ac.uk including the URL of the record and the reason for the withdrawal request.



eprints@whiterose.ac.uk
<https://eprints.whiterose.ac.uk/>



RESEARCH ARTICLE

10.1002/2014PA002625

Key Points:

- New Pliocene East Antarctic IRD record and iceberg trajectory-melting model
- Increase in remotely sourced IRD between ~3.27 and ~2.65 Ma due to cooling SSTs
- Evidence for ice sheet retreat in the Aurora Basin during interglacials

Supporting Information:

- Readme
- Text S1 and Tables S1–S3

Correspondence to:

C. P. Cook,
c.cook@ufl.edu

Citation:

Cook, C. P., et al. (2014), Sea surface temperature control on the distribution of far-traveled Southern Ocean ice-rafted detritus during the Pliocene, *Paleoceanography*, 29, 533–548, doi:10.1002/2014PA002625.

Received 5 FEB 2014

Accepted 5 MAY 2014

Accepted article online 8 MAY 2014

Published online 12 JUN 2014

Sea surface temperature control on the distribution of far-traveled Southern Ocean ice-rafted detritus during the Pliocene

C. P. Cook^{1,2,3}, D. J. Hill^{4,5}, Tina van de Flierdt³, T. Williams⁶, S. R. Hemming^{6,7}, A. M. Dolan⁴, E. L. Pierce⁸, C. Escutia⁹, D. Harwood¹⁰, G. Cortese¹¹, and J. J. Gonzales⁹

¹Grantham Institute for Climate Change, Imperial College London, London, UK, ²Now at Department of Geological Sciences, University of Florida, Gainesville, Florida, USA, ³Department of Earth Sciences and Engineering, Imperial College London, London, UK, ⁴School of Earth and Environment, University of Leeds, Leeds, UK, ⁵British Geological Survey, Nottingham, UK, ⁶Lamont-Doherty Earth Observatory, Palisades, New York, USA, ⁷Department of Earth and Environmental Sciences, Columbia University, Lamont-Doherty Earth Observatory, Palisades, New York, USA, ⁸Department of Geosciences, Wellesley College, Wellesley, Massachusetts, USA, ⁹Instituto Andaluz de Ciencias de la Tierra, CSIC-UGR, Armilla, Spain, ¹⁰Department of Geology, University of Nebraska–Lincoln, Lincoln, Nebraska, USA, ¹¹Department of Paleontology, GNS Science, Lower Hutt, New Zealand

Abstract The flux and provenance of ice-rafted detritus (IRD) deposited in the Southern Ocean can reveal information about the past instability of Antarctica's ice sheets during different climatic conditions. Here we present a Pliocene IRD provenance record based on the ⁴⁰Ar/³⁹Ar ages of ice-rafted hornblende grains from Ocean Drilling Program Site 1165, located near Prydz Bay in the Indian Ocean sector of the Southern Ocean, along with the results of modeled sensitivity tests of iceberg trajectories and their spatial melting patterns under a range of sea surface temperatures (SSTs). Our provenance results reveal that IRD and hence icebergs in the Prydz Bay area were mainly sourced from (i) the local Prydz Bay region and (ii) the remote Wilkes Land margin located at the mouth of the low-lying Aurora Subglacial Basin. A series of IRD pulses, reaching up to 10 times background IRD flux levels, were previously identified at Site 1165 between 3.3 and 3.0 Ma. Our new results reveal that the average proportion of IRD sourced from distal Wilkes Land margin doubles after 3.3 Ma. Our iceberg trajectory-melting models show that slower iceberg melting under cooling SSTs over this middle Pliocene interval allowed Wilkes Land icebergs to travel farther before melting. Hence, declining SSTs can account for a large part of the observed IRD provenance record at Site 1165. In early Pliocene IRD layers, sampled at suborbital resolution around 4.6 Ma, we find evidence for significant increases in icebergs derived from Wilkes Land during very warm interglacials. This is suggestive of large-scale destabilization of the East Antarctic Ice Sheet in the Aurora Subglacial Basin, as far-traveled icebergs would have to overcome enhanced melting in warmer SSTs. Our results highlight the importance of considering SSTs when interpreting IRD flux and provenance records in distal locations.

1. Introduction

The abundance and provenance of ice-rafted detritus (IRD) in marine sediments have been recognized as useful tools in constraining past ice sheet histories [e.g., Hemming, 2004, and references therein]. This is because the flux of outlet glaciers, and hence iceberg production rates, will vary significantly during changes in ice sheet volume and/or ice thickness at grounding lines [Schoof, 2007]. Particularly in the North Atlantic, geochemical IRD provenance studies have revealed valuable evidence for the spatial and temporal history of rapid and large-scale destabilization of Northern Hemisphere continental ice sheets over timescales of thousands to millions of years [e.g., Hemming, 2004; Peck et al., 2007; Downing and Hemming, 2012; Bailey et al., 2012, 2013; Thierens et al., 2012].

The most significant late Pleistocene Northern Hemisphere IRD depositional events occurred during cold intervals (i.e., Heinrich events) [Hemming, 2004] and are relatively well understood in terms of the locations of ice sheet instability based on provenance studies. Comparatively, Neogene IRD records from the Southern Ocean are sparse, despite the need to better understand the sensitivity of Antarctica's much larger ice sheets to climatic change. Approximately 58 m of sea level equivalent of ice is present today on the Antarctic continent [Fretwell et al., 2013], in comparison to only ~7 m of sea level equivalent on Greenland [Bamber et al., 2001]. Southern Ocean IRD records and derived interpretations about ice sheet history have therefore been directed at periods characterized by climatic warmth, such as the Pliocene Epoch [e.g., Williams et al., 2010; Passchier, 2011; Patterson et al., 2011].

The early Pliocene (5.33 to 3.60 Ma) was a time of regional warmth in Antarctica, with seasonal sea surface temperatures (SSTs) between 1 and 7°C warmer than modern [Bohaty and Harwood, 1998; Whitehead and Bohaty, 2003; Escutia et al., 2009; McKay et al., 2012; Clark et al., 2013]. Marine sediments, deposited around the perimeter of the Antarctic continent, carry a clear record of ice loss from Antarctica's ice shelves and ice sheets in response to these warm spring and summer temperatures [e.g., Whitehead et al., 2006; O'Brien et al., 2007; Naish et al., 2009; Bart and Iwai, 2012; Cook et al., 2013].

To further investigate ice sheet change during this time, Passchier [2011] carried out a detailed investigation of the Pliocene (5.33 to 2.58 Ma) history of ice-rafted deposition in East Antarctica using IRD mass accumulation rates (MAR) at Ocean Drilling Program (ODP) Site 1165 (64°22'S, 67°13'E), in Prydz Bay. This record revealed highly variable IRD supply to the site throughout the Pliocene, interpreted as evidence for a dynamic grounding line in the Prydz Bay area [Passchier, 2011]. A key feature of the record is a tenfold increase in IRD MAR after marine isotope stage M2 glacial (~3.3 Ma) [Passchier, 2011] (Figure 2). This increase has been interpreted as evidence for cooling SSTs and increased iceberg production in the Prydz Bay area associated with regional ice sheet growth after the comparative warmth of the early Pliocene [Passchier, 2011].

In a pioneering study, Williams et al. [2010] traced the provenance of five Pliocene IRD layers deposited at ~4.65 and ~3.5 Ma at the same site using the $^{40}\text{Ar}/^{39}\text{Ar}$ ages of ice-rafted hornblende grains. They identified Pliocene IRD deposited at Site 1165 was not only supplied from the local Prydz Bay area but in fact also from the distal Wilkes Land margin, over 1500 km to the east, suggesting processes other than local ice sheet dynamics controlled IRD deposition at Site 1165 through time. Airborne geophysical surveys and ice sheet modeling suggest that Miocene/Pliocene ice retreat in East Antarctica may have been most pronounced in low-lying continental depressions such as the Wilkes Subglacial Basin and the larger neighboring Aurora Subglacial Basin in Wilkes Land [Hill et al., 2007; Dolan et al., 2011; Young et al., 2011] (see Figure 1 for the location of the latter). Evidence for large-scale ice sheet retreat in the Wilkes Subglacial Basin during the early Pliocene has recently been provided by Cook et al. [2013] based on the study of fine-grained sediment provenance at IODP Site U1361 (64°24'S, 143°53'E).

However, the record presented by Cook et al. [2013] as well as the previously published IRD record at Site 1165 [Williams et al., 2010] does not extend into the cooler middle and late Pliocene. Few Southern Ocean SST records extend from the warm early Pliocene to the cooler late Pliocene [Bohaty and Harwood, 1998; see Clark et al., 2013], but TEX_{86}^L data from the Ross Sea [McKay et al., 2012] show a decline in summer and spring temperatures from 2–5°C above modern during the early Pliocene to 0–2°C after ~3.3 Ma. This decline in temperature regionally is coincident with the significant increase in IRD MAR recorded at Site 1165 [Passchier, 2011] and implies that SSTs could have played an important role in Pliocene changes in IRD deposition at Site 1165.

To quantitatively investigate the relationship between variable SSTs and IRD deposition in the Southern Ocean during the Pliocene, we here revisit Site 1165 and significantly expand upon the study of Williams et al. [2010] by combining new insights into the location of iceberg calving sites in East Antarctica with sensitivity simulations of a thermodynamic iceberg model under different SST scenarios. Our results suggest that IRD studies under warm climatic conditions may indeed reveal evidence for ice sheet instabilities in far-field locations but that warmer ocean temperatures can have a profound effect on iceberg survivability and need to be taken into account when interpreting IRD records.

2. Using $^{40}\text{Ar}/^{39}\text{Ar}$ Ages of Ice-Rafted Hornblende Grains From ODP Site 1165 to Constrain Past Sites of Iceberg Calving

The $^{40}\text{Ar}/^{39}\text{Ar}$ dating of ice-rafted (>150 μm) hornblende grains can serve as a powerful approach to locate the continental sources of past iceberg production. The underlying rationale is that ice-rafted detrital mineral grains, identified in marine sediments, can contain information about the thermochronological history of their continental source areas. For example, the $^{40}\text{Ar}/^{39}\text{Ar}$ age of a detrital hornblende grain reflects the time since it formed or cooled below ~500°C [McDougall and Harrison, 1999], a temperature that typically marks the last major tectonometamorphic event to have affected its continental bedrock source. A geologically diverse and polymetamorphic continent such as Antarctica is characterized by a large range in hornblende $^{40}\text{Ar}/^{39}\text{Ar}$ ages

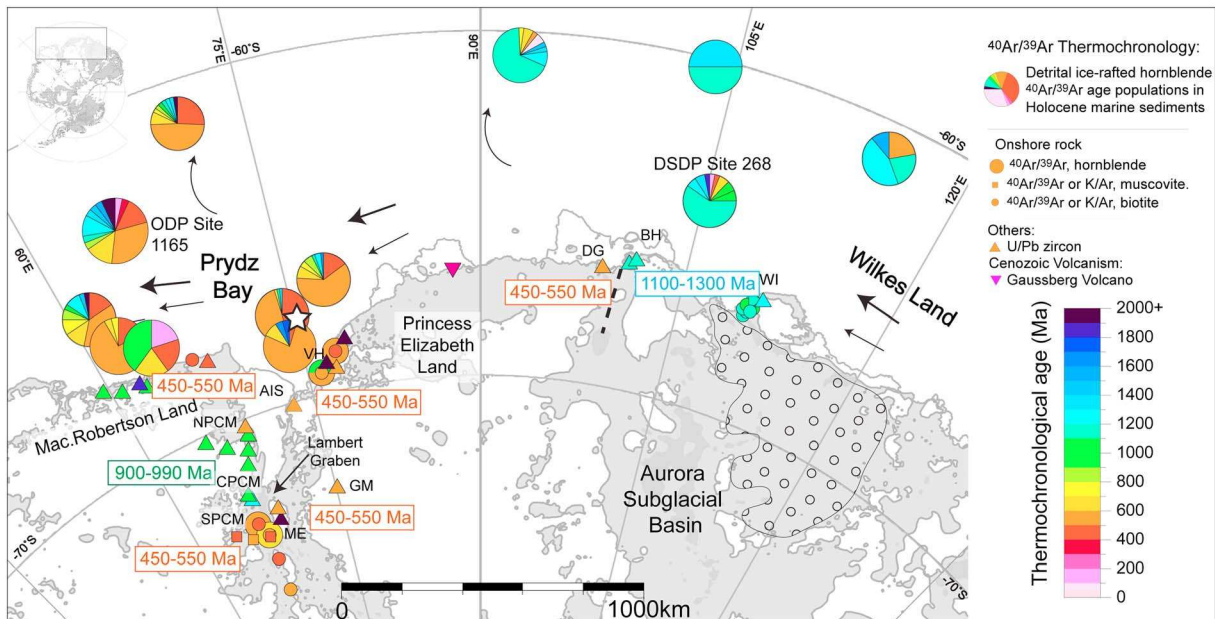


Figure 1. Map of study area and regional continental thermochronology. Onshore data are based on $^{40}\text{Ar}/^{39}\text{Ar}$ ages of individual hornblende and mica grains and U-Pb dating of zircons (modified from Williams et al. [2010]); data are from Black and James [1983], Black et al. [1991], Young and Black [1991], Sheraton et al. [1992, 1993], Takigami et al. [1992], Post et al. [1996], Young et al. [1997], Jacobs et al. [1998, 2003], Carson et al. [2000], Boger et al. [2002], Fitzsimons [2000a, 2000b], Tong et al. [2002], Halpin et al. [2007], Liu et al. [2006, 2007], Wilson et al. [2007], Phillips et al. [2007], and Corvino et al. [2008, 2011]. Values shown in boxes represent the age ranges for the most recent major tectonic event in different areas. The stipple line around 100°E marks the geological boundary between older overprint ages to the east (i.e., Wilkes Land) and younger ages in the Prydz Bay area to the west [Clarke et al., 1995; Clark et al., 2000; Boger, 2011]. Shading on the continent outlines the modern subglacial topography from BEDMAP 2 [Fretwell et al., 2013] with white areas marking highlands and grey areas marking areas below sea level. Shaded region within the Aurora Subglacial Basin represents inferred open marine areas during Neogene ice sheet retreat events [Young et al., 2011]. Offshore data are based on $^{40}\text{Ar}/^{39}\text{Ar}$ ages of individual hornblende grains from Holocene marine sediments [Roy et al., 2007; Brachfeld et al., 2007; Williams et al., 2010; Pierce et al., 2011; this study]. Arrows offshore indicate the approximate transport regions and pathways of icebergs (Antarctic Iceberg Tracking Database [1978–2012]; available at <http://www.scp.byu.edu/data/iceberg/database1.html>). Larger arrows represent the highest concentration of icebergs, along trajectories where surface currents are strongest. The white star shows the location of ODP Site 739. NPCM: Northern Prince Charles Mountains, CPCM: Central Prince Charles Mountains, SPCM: Southern Prince Charles Mountains, ME: Mawson Escarpment, GM: Grove Mountains, AIS: Amery Ice Shelf, VH: Vestfold Hills, GA: Gaussberg Volcanic field, DG: Denman Glacier, BH: Bunger Hills, and WI: Windmill Islands.

[e.g., Roy et al., 2007; Pierce et al., 2011]. Figure 1 highlights the two main geographical provenance sectors between 60° and 120°E in East Antarctica. A more detailed description of the continental geology and regional thermochronology relevant to Site 1165 is provided in Williams et al. [2010]. The two sectors are the following:

1. The Prydz Bay sector (~60°E to ~100°E; hornblende $^{40}\text{Ar}/^{39}\text{Ar}$ ages of ~550–450 Ma): bedrock exposed in Mac.Robertson Land, the central and southern Prince Charles Mountains, the Mawson Escarpment, the Grove Mountains, the eastern flank of the Lambert Graben, and the Princess Elizabeth Land coast. All areas were significantly overprinted and/or formed during the Paleozoic Pan-African Orogeny [e.g., Boger et al., 2011].
2. The Wilkes Land sector (east of ~100°E; hornblende $^{40}\text{Ar}/^{39}\text{Ar}$ ages of ~1350–1100 Ma): bedrock exposed along the Wilkes Land margin to the east of the Denman Glacier, which shows a regionally distinct age range characteristic of the Mesoproterozoic Grenville Orogeny [e.g., Boger et al., 2011]. This source area is located at a considerable distance from Site 1165 in the Prydz Bay region (>1500 km) and is associated with the low-lying Aurora Subglacial Basin [Pierce et al., 2011] (Figure 1).

Importantly, IRD provenance in Holocene core-top sediments shows that the Prydz Bay signature dominates the IRD signal offshore of Prydz Bay, and likewise for other provenance sectors around the Antarctic margin, indicating that IRD is not usually transported far from its source under today's climatic conditions [Brachfeld et al., 2007; Roy et al., 2007; Williams et al., 2010; Pierce et al., 2011; this study] (Figure 1). In contrast, increased relative levels of far-traveled IRD, from Wilkes Land and sites farther to the east, were observed in Pliocene and late Miocene IRD layers at Site 1165 [Williams et al., 2010], which imply increased output of IRD-bearing icebergs from glaciers in these region during their deposition.

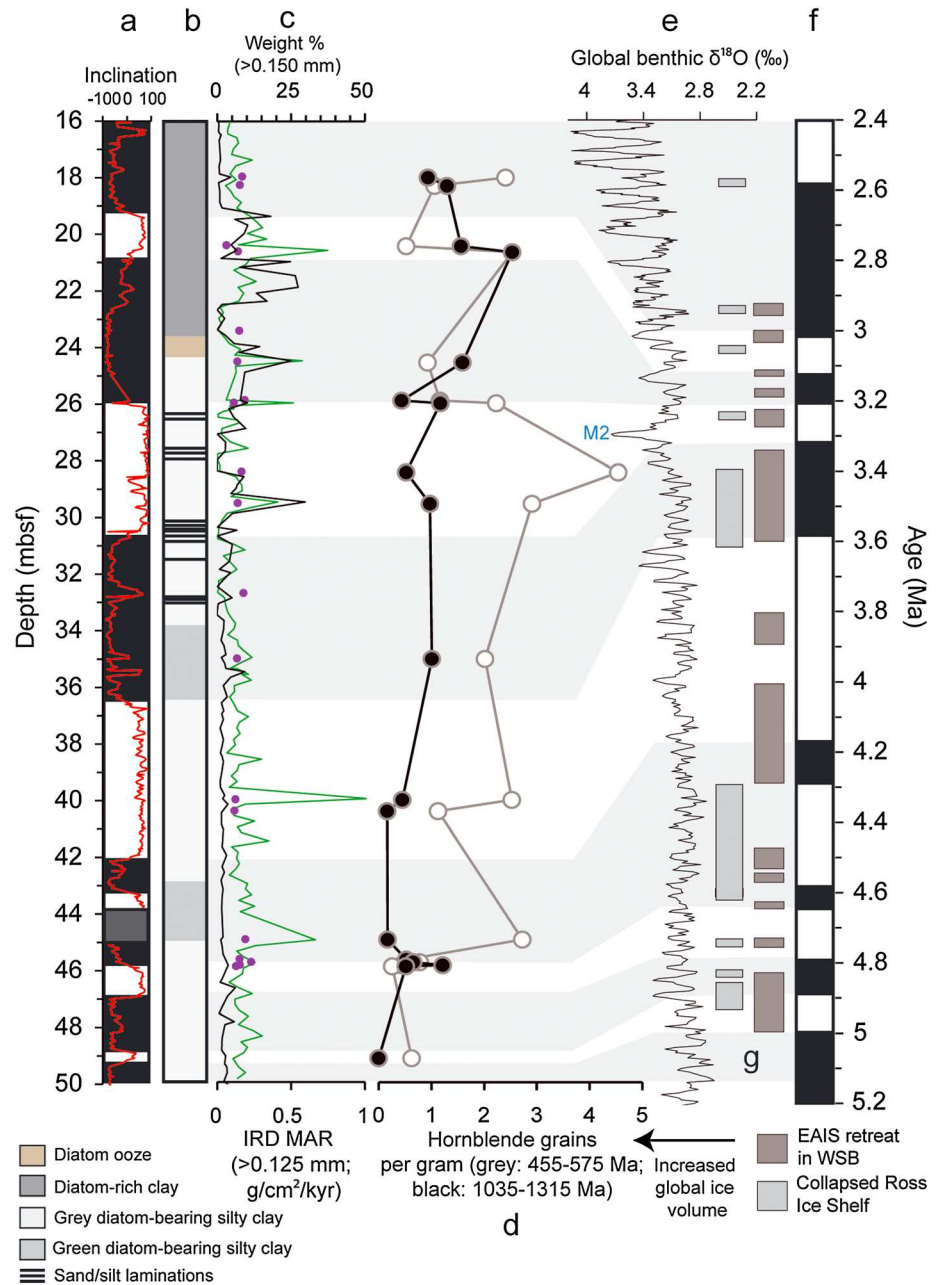


Figure 2. Downcore summary of Pliocene sediments from ODP Site 1165. (a) paleomagnetic chron boundaries [Florindo *et al.*, 2003] with inclination data shown in red and grey shading indicating areas with no data; (b) lithostratigraphy (modified after Passchier [2011]); (c) green: weight % of fractions >150 μm [Warnke *et al.*, 2004] and black: ice-rafted mass accumulation rates calculated for detrital fractions (>125 μm) (IRD MAR = weight % >125 μm \times terrigenous fraction \times bulk density \times linear sedimentation rate; from Passchier [2011], see addendum at <http://doi.pangaea.de/10.1594/PANGAEA.832115>), purple data points: weight % of >150 μm fractions of samples analyzed for IRD provenance in this study; (d) number of hornblende grains per gram of bulk sediment for the two most significant and distinct hornblende $^{40}\text{Ar}/^{39}\text{Ar}$ age populations (grey: 455–575 Ma and black: 1035–1315 Ma); (e) global benthic oxygen isotope stack [Lisiecki and Raymo, 2005], M2: glacial marine isotope stage M2; (f) paleomagnetic chron boundaries from Gradstein *et al.* [2012]; (g) intervals of East Antarctic Ice Sheet (EAIS) retreat in the Wilkes Subglacial Basin (WSB) [Cook *et al.*, 2013; Cook, 2013] and intervals of diatomite deposition in the Ross Sea indicating open ocean conditions and retreat of the Ross Ice Shelf [Naish *et al.*, 2009].

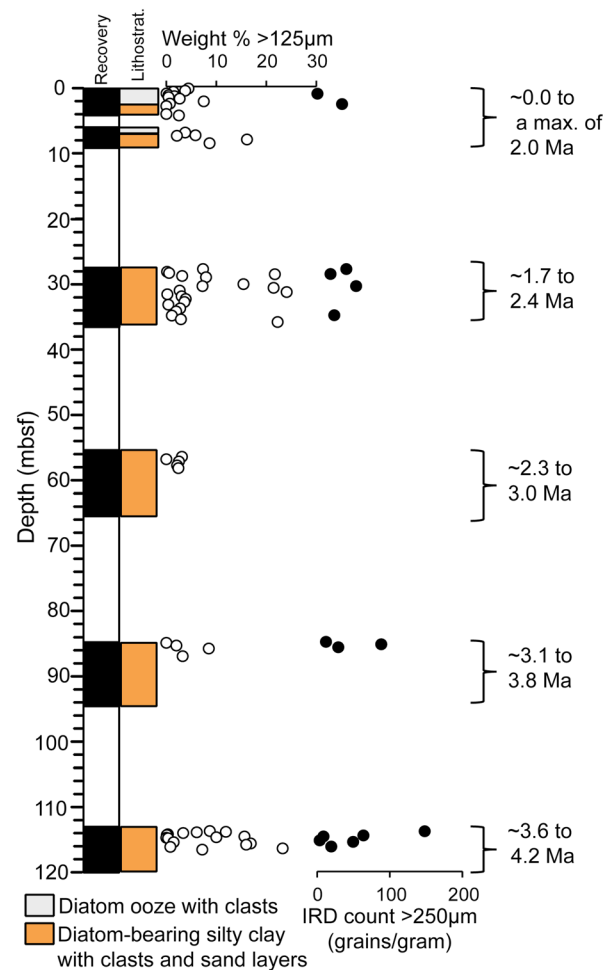


Figure 3. Downcore summary of Pliocene and Quaternary sediments from DSDP Site 268. From left to right: (i) depth in meters below sea floor; (ii) coring recovery, with black indicating recovery of sediments and white indicating intervals of no recovery; (iii) lithostratigraphy (modified after Hayes et al. [1975]); (iv) weight abundance of >125 µm detrital fractions; (v) IRD grain counts (grains >250 µm per gram); and (vi) estimated ages of recovered sediments based on radiolarian and diatom biozones (see supporting information).

3. Study Sites and Sampling

Ocean Drilling Program Site 1165 was drilled in 3537 m water depth and is located in the Indian sector of the Southern Ocean, ~400 km northwest of Prydz Bay and ~1500 km to the west of the western segment of the Wilkes Land margin, inland of which lies the Aurora Subglacial Basin [Young et al., 2011]. Today, katabatic winds blowing off the continental interior of the East Antarctic Ice Sheet (EAIS) drive the Antarctic coastal current, which carries icebergs in a counterclockwise direction around the continent (Figure 1) [e.g., Stuart and Long, 2011]. Today, Site 1165 lies in the pathway of icebergs sourced from the proximal Prydz Bay region and sites to the east.

The top ~50 m of Site 1165 is composed of diatom-bearing silty clays with silt laminations, diatom ooze, and diatom-rich clays, providing a Pliocene and Pleistocene record of hemipelagic, turbidity current, and ice-rafted deposition [Warnke et al., 2004] (Figure 2). The age model of Site 1165 is based on magnetostratigraphic data supported by biostratigraphy [Florindo et al., 2003] and is identical to the one used and described by Passchier [2011], with the studied Pliocene section representing ~2.7 million years of deposition between 5.2 and 2.5 Ma. Linear sedimentation rates based on the age model of Florindo et al. [2003] do not capture likely differences in sedimentation between deposition of hemipelagic and turbidite-related sediments. A significant change in sedimentation at Site 1165 occurred around 3.3 Ma [Warnke et al., 2004]. According to the existing age model [Florindo et al., 2003], this change is marked by an increase in

sedimentation rates and an increase in clay-sized material, possibly related to increased turbidite sedimentation and accompanied by a significant increase in ice-rafted deposition [Passchier, 2011] (Figure 2).

Twenty-one IRD layers were selected from Site 1165 for hornblende $^{40}\text{Ar}/^{39}\text{Ar}$ age analyses, using published grain size [Grutzner et al., 2003; Warnke et al., 2004] and IRD MAR [Passchier, 2011] records in order to sample intervals of high and low IRD delivery (Figure 2). Linear sedimentation rates reveal that each 2 cm thick core sample could represent up to 5500 years of deposition. One core-top sample, two Pleistocene samples (7.00 m below seafloor (bsf) and 14.75 m bsf), and 18 Pliocene samples were selected in total from Site 1165. Between 46.00 and 45.50 m bsf, four samples were selected for IRD provenance analysis, in order to increase the resolution of samples over this interval previously studied by Williams et al. [2010] and to sample potential orbital-scale variability.

To monitor IRD supply from the Wilkes Land margin during the Pliocene, sediments from Deep Sea Drilling Project (DSDP) Site 268 (63°56'S, 105°09'E) (Figure 1), located offshore of the Bunger Hills (Wilkes Land margin, Figure 1), were studied for grain size and IRD provenance. The site was spot cored in 3544 m water depth, and only ~66 m of Oligocene to Quaternary sediments were recovered from ~474 m of penetration (14% recovery) [Hayes et al., 1975] (Figure 3). Sediments above ~160 m (Unit 1 of Hayes et al. [1975]) are

Table 1. Hornblende $^{40}\text{Ar}/^{39}\text{Ar}$ Age Ranges From ODP Site 1165 and DSDP Site 268 ($>150\ \mu\text{m}$)

	Depth (m bsf)	Age (Ma)	0–410 Ma	455–575 Ma	580–1030 Ma	1035–1315 Ma	>1315 Ma	Total
ODP Site 1165:								
1H 1W 1–3 cm	0.01	0.00	2	12	5	5	4	28
2H 2W 20–22 cm	7.00	1.00	0	20	4	10	0	34
2H 6W 45–47 cm	14.75	1.60	0	12	2	10	3	27
3H 2W 15–17 cm	17.95	2.7	0	18	3	7	4	32
3H 2W 45–47 cm	18.25	2.80	1	9	5	11	1	27
3H 3W 109–112 cm	20.39	3.09	1	4	6	12	1	24
3H 3W 130–132 cm	20.60	3.11	0	8	9	8	1	26
3H 6W 70–73 cm	24.50	3.19	0	7	3	12	6	28
4H 1W 6–9 cm	25.86	3.205	0	8	3	3	2	16
4H 1W 15–17 cm	25.95	3.207	0	21	6	11	4	42
4H 2W 109–112 cm	28.39	3.27	0	26	11	3	2	42
4H 3W 70–72 cm	29.50	3.30	0	24	5	8	4	41
4H 6W 80–82 cm ^a	34.10	3.48	0	14	12	10	3	39
4H 7W 20–22 cm	35.00	3.53	0	18	8	9	0	35
5H 4W 20–22 cm	40.00	3.96	0	17	6	6	3	32
5H 4W 60–62 cm	40.40	4.01	1	7	8	7	1	24
6H 1W 15–17 cm	44.95	4.55	0	16	7	0	1	24
6H 1W 70–72 cm ^a	45.50	4.60	3	19	8	5	4	39
6H 1W 84–86 cm	45.64	4.62	0	5	1	5	1	12
6H 1W 90–92 ^a	45.70	4.63	0	31	21	5	9	66
6H 1W 94–96 cm	45.74	4.64	1	6	4	5	3	19
6H 1W 100–102 cm ^a	45.80	4.65	0	14	8	4	15	41
6H 1W 104–106 cm	45.84	4.655	0	9	7	3	1	20
6H 1W 110–112 cm	45.90	4.665	0	2	4	4	2	12
6H 1W 121–123 cm ^a	46.00	4.75	1	16	6	2	2	27
6H 3W 135–137 cm	49.15	4.99	0	4	0	0	0	4
Total			9	347	162	165	77	761
DSDP Site 268:								
			0–660 Ma	660–675 Ma	675–1100 Ma	1100–1280 Ma	1280–1840 Ma	Total
1R 1W 72–74 cm ^a	0.72		3	1	4	21	3	32
3R 2W 81–82 cm	57.81	2.3	1	8	3	45	6	63
5R 1W 88–89 cm	114.38	4.2	1	0	2	35	6	44
Total			5	9	9	101	15	139

^aFrom Williams et al. [2010].

composed of diatom oozes, silty clays, and clays with abundant sand and pebbles throughout [Piper and Brisco, 1975], interpreted to represent hemipelagic and terrigenous turbidity-related deposition with common iceberg rafting. The age of sediments from the first five cored sections of Unit 1 of DSDP Site 268 is revisited here to provide an updated assessment based on new radiolarian and diatom biostratigraphic data (see supporting information; based on McCollum [1975] and Cortese and Gersonde [2008]). Core 5 (117.00 to 113.50 m bsf) was deposited within the time interval ~4.2 to 3.6 Ma, Core 4 (94.50 to 85.00 m bsf) within the interval between ~3.8 and 3.1 Ma, Core 3 (66.00 to 56.50 m bsf) within the interval of ~3.0 to 2.3 Ma, and Core 2 (37.50 to 28.00 m bsf) was deposited within time interval ~2.4 and 1.7 Ma. Core 1 (9.00 to 0.00 m bsf) represents the time interval between ~2.0 and 1.2 Ma, based on radiolarian data, and <0.62 Ma from diatom data. Sixty-five samples were selected for grain size analysis from these five core intervals (Figure 3), and IRD counts were carried out on 17 samples with material >250 μm in size. Of the available Pliocene samples with material >150 μm in size, two were selected for hornblende provenance analyses.

4. Methodology

Bulk sediment samples from Site 1165 were wet sieved, whereas sediments from Site 268 were leached of organic material using 10% hydrogen peroxide, sodium polyphosphate and 1M HCl, and subsequently analysed using a Laser Diffraction Particle Size Analyzer (Coulter LS230) at the University of Barcelona, Spain. Ice-rafted mineral grains of the amphibole hornblende were handpicked from the >150 μm fractions and analyzed for

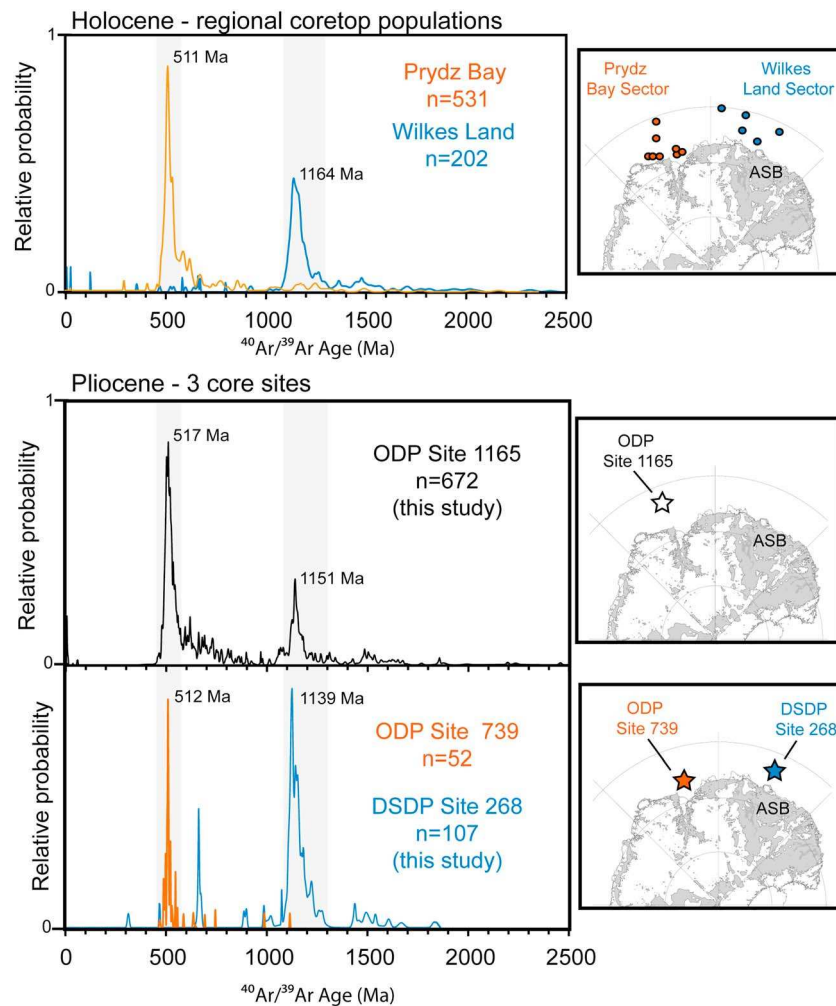


Figure 4. Comparison of modern and Pliocene IRD provenance fingerprints offshore Prydz Bay and Wilkes Land. (top) The modern day as derived from 12 core locations and their ice-rafted hornblende $^{40}\text{Ar}/^{39}\text{Ar}$ age populations [Brachfeld et al., 2007; Roy et al., 2007; Pierce et al., 2011; this study]. (bottom) Pliocene results for three different sites: ODP Site 1165 (this study and Williams et al. [2010]) (top) and DSDP Site 268 (this study) and ODP Site 739 [Tochilin et al., 2012] (bottom) graph. All relative probability and weighted means of the $^{40}\text{Ar}/^{39}\text{Ar}$ age distributions of individual $>150\ \mu\text{m}$ hornblende grains were calculated using ISOPLLOT [Ludwig, 2003].

their $^{40}\text{Ar}/^{39}\text{Ar}$ ages. Individual hornblende grains and monitor standards (McLure Mountain hornblende (MMhb)) were irradiated at the Training, Research, Isotopes, General Atomic reactor at the U.S. Geological Survey in Denver with cadmium shielding. $^{40}\text{Ar}/^{39}\text{Ar}$ ages were obtained using single-step CO_2 laser fusion at the Lamont-Doherty Earth Observatory argon geochronology lab (Argon Geochronology for the Earth Sciences). J values used to correct for neutron flux were calculated using the coirradiated MMhb standard with an age of 525 Ma [Samson and Alexander, 1987]. Measured values were corrected for blanks and mass discrimination using measurements of atmospheric argon from an air pipette. Isotopes were also corrected for nuclear interferences based on reported production rates [Dalrymple et al., 1981]. Analytical uncertainties are based on the internal precision of measurements and variation of Mmhb values and are less than 2%. Our new data set is supplemented by five samples previously reported by Williams et al. [2010] and which are also included in Table 1.

5. Results

Sediments from Site 1165 yielded between four and 36 hornblende grains per sample (0.6 to 5.1 grains per gram of sediment), with no obvious trend in hornblende abundance upcore. Hornblende grains analyzed were characterized by two distinct $^{40}\text{Ar}/^{39}\text{Ar}$ age populations (Tables 1 and S2 and Figures 2 and 4). The first

ranges from 455 to 575 Ma and is composed of 253 grains (out of a total of 549; ~46%), with 207 of these grains (~90%) dated between 480 and 550 Ma and a weighted mean age of 517 Ma. The second age population ranges between 1035 and 1315 Ma and is composed of 165 grains (~25%), with 77 grains (~60%) between 1120 and 1175 Ma and a weighted mean age of 1151 Ma. This latter population occurs in highest abundances during intervals of higher sedimentation rates after ~3.27 Ma and around 4.6 Ma, although these intervals (and another interval around 5 Ma) also contain several samples with none or little grains with ages between 1035 and 1315 Ma. Outside of these two main age populations, remaining hornblende grains yielded $^{40}\text{Ar}/^{39}\text{Ar}$ ages from 10 to 410 Ma (6 grains, ~1%) and dispersed ages ranging from 580 to 1035 Ma (162 grains in total, ~21.2%) to >1325 Ma (44 grains in total, ~8%).

Results of grain size analyses from DSDP Site 268 (Figure 3) reveal that sediments are dominated by <63 μm fractions (average 87.7 wt %), with smaller amounts of material between 63 and 125 μm (average 5.7 wt %), 125 to 250 μm (average 4.9 wt %), and >250 μm (average 2.1 wt %). Counts of IRD grains >250 μm in size from 17 samples range from 1 to 49 (0.4 to 148.1 grains per gram of sediment), revealing significantly higher concentrations of IRD grains than at Site 1165. There is no obvious change in the relative abundance of grain size fractions upcore.

Hornblende grains extracted from Pliocene DSDP Site 268 sediments are dominated by $^{40}\text{Ar}/^{39}\text{Ar}$ ages between 1100 and 1280 Ma (Figure 4), with 79 grains of 107 in total (~73%) falling within this age range (Tables 1 S3), producing a weighted mean age of 1139 Ma. Remaining hornblende grains show $^{40}\text{Ar}/^{39}\text{Ar}$ ages between 660 and 675 Ma (8 grains of 107, 7.4%), 675 and 1100 Ma (7 grains, 6.5%), 1280–1840 Ma (11 grains of 107, 10.2%), and 313 ± 4 and 468 ± 2 Ma (two grains).

6. Provenance of Ice-Rafted Hornblendes

Comparison of our new $^{40}\text{Ar}/^{39}\text{Ar}$ hornblende age results with existing provenance constraints (see section 2) reveals that ice-rafted hornblende grains deposited at Site 1165 were sourced from both the Prydz Bay sector ($^{40}\text{Ar}/^{39}\text{Ar}$ age range of 455–575 Ma; 46% of all Pliocene grains analyzed) and the Wilkes Land sector (1035–1315 Ma; 25% of all Pliocene grains), in good agreement with the findings described by *Williams et al.* [2010]. Ages that fall within the third largest age range (580–1035 Ma; 21% of all grain analyzed) are also present in regional Prydz Bay core-top sediments (Figure 4). Poor onland exposure of these ages limits robust provenance tracing. We therefore refrain from interpreting such ages and instead focus on the two main age populations delineated above.

Supporting evidence for identification of the Prydz Bay area and the Wilkes Land margin as the two main sources for ice-rafted hornblende grains can be taken from the $^{40}\text{Ar}/^{39}\text{Ar}$ ages of ice-rafted hornblende grains in Pliocene sediments deposited at other sites directly offshore of these regions (Figure 4). Paleozoic $^{40}\text{Ar}/^{39}\text{Ar}$ hornblende grain ages (450–550 Ma) dominate the provenance of Pliocene sediments at ODP Site 739 (67°16'87"S, 75°04'91"E), located offshore of the Lambert Glacier, closer to the continent than Site 1165 [*Tochilin et al.*, 2012]. Notably, Pliocene sediments from Site 739 show no evidence for Mesoproterozoic $^{40}\text{Ar}/^{39}\text{Ar}$ hornblende ages (Figure 4), suggesting the Prydz Bay area was an unlikely source for ice-rafted hornblende grains with these ages. Furthermore, hornblende grains in Pliocene sediments deposited offshore the Wilkes Land continental margin, at DSDP Site 268, are dominated by Mesoproterozoic $^{40}\text{Ar}/^{39}\text{Ar}$ ages (1100–1300 Ma) (Figure 4). Therefore, we conclude that the Wilkes Land margin was the most likely source of hornblende grains in Site 1165 sediments with $^{40}\text{Ar}/^{39}\text{Ar}$ ages between ~1100 and ~1300 Ma.

7. Sea Surface Temperature Control on the Melting Patterns of Far-Traveled Icebergs

If we assume that the Wilkes Land and Prydz Bay-derived IRD provenance populations account for 100% of all IRD (i.e., excluding all hornblende grains with $^{40}\text{Ar}/^{39}\text{Ar}$ ages outside of the 455–575 Ma and 1035–1315 Ma ranges), we can calculate the relative abundances of both of these populations (Figures 2 and 4) [see also *Williams et al.*, 2010], which vary through time. The Prydz Bay sector accounts for 49% of grains deposited between 5 and ~3.27 Ma and 38% of grains between ~3.2 and ~2.65 Ma. This population is variable in abundance throughout our studied Pliocene section (total range between ~17 and 100%). Conversely, while the relative abundance of Wilkes Land-derived hornblende grains is overall lower than the Prydz Bay abundance (0 to 50%), a distinct increase in Wilkes Land-supplied hornblendes is evident in sediments deposited between ~3.2 and 2.65 Ma. The average contribution of these grains accounts for 18% out of all grains deposited between ~5 and 3.27 Ma and

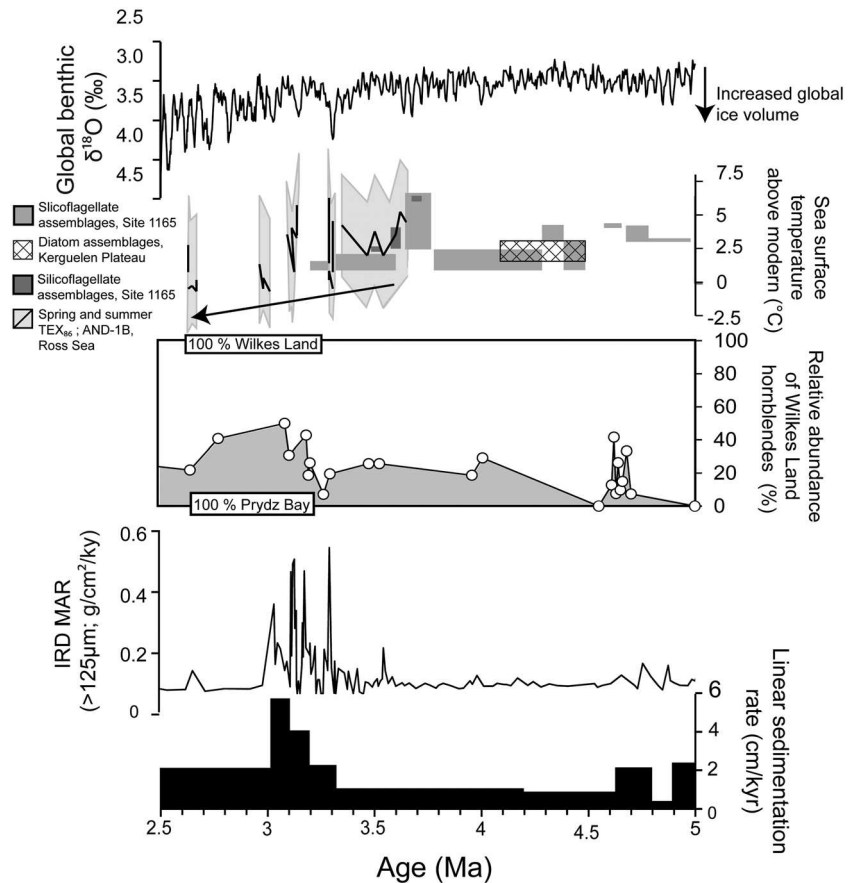


Figure 5. Summary of studied Pliocene section from Site 1165 and comparison to regional and global records. From bottom to top: (i) linear sedimentation rate: small increases in sedimentation rates around ~4.6 Ma and ~5 Ma have been attributed to cyclical variations in grain size associated with contourite deposits [Passchier, 2011]; (ii) IRD MAR [Passchier, 2011]; (iii) abundance of Wilkes Land hornblende grains relative to all other grains; (iv) numerous regional seasonal SST estimates from Site 1165 (diatom and silicoflagellate assemblages; [Whitehead and Bohaty, 2003] light grey boxes and [Escutia et al., 2009] dark grey boxes) and the Kerguelen Plateau (diatom assemblages, [Bohaty and Harwood, 1998] hatched boxes); (v) Ross Sea (black line and grey uncertainty range) spring and summer upper water column temperatures; TEX₈₆^L [McKay et al., 2012]; and (vi) global benthic oxygen isotope stack [Lisiecki and Raymo, 2005].

~33% between ~3.2 and 2.65 Ma. An increase in Wilkes Land IRD is also evident in several IRD layers sampled at high resolution around ~4.6 Ma, contemporaneous with increased sedimentation rates (Figure 5).

Locally derived Prydz Bay IRD would be expected to dominate sediments at Site 1165, relative to IRD supplied from remote locations, due to the closer proximity of the Prydz Bay source area, and this is what we observe in our provenance data. Increased linear sedimentation rates, the increased delivery of clays [Warnke, 2004], and increased depositional rates of IRD at Site 1165 after ~3.3 Ma [Passchier, 2011] appear to be more or less contemporaneous with an observed relative increase in Wilkes Land-derived hornblende grains after ~3.27 Ma.

Expansion of the Lambert Glacier and accompanying tributary glaciers during the late Pliocene has been documented in the Prydz Bay area from seismic surveys and sedimentological changes of continental shelf and slope sediments [Rebesco et al., 2006; O'Brien et al., 2007; Volpi et al., 2009], and expansion of the west Antarctic ice sheet is evident in increased deposition of glacial marine sediments in the Ross Sea [Naish et al., 2009; McKay et al., 2012]. Advance of the ice sheet margin in Prydz Bay at this time could explain the increased supply of turbidite sediments to Site 1165 [Passchier, 2011] (Figure 2) as well as the significant increase in IRD MAR observed during the late Pliocene. Ice sheet calving margins would be located closer to our study site as they advanced onto the continental shelf [O'Brien et al., 2007], and more debris-rich icebergs could be produced during periodic deglaciations following large glacial expansion events such as marine isotope stage M2 (Figure 2). However, our observation of an overall average increase in the abundance of

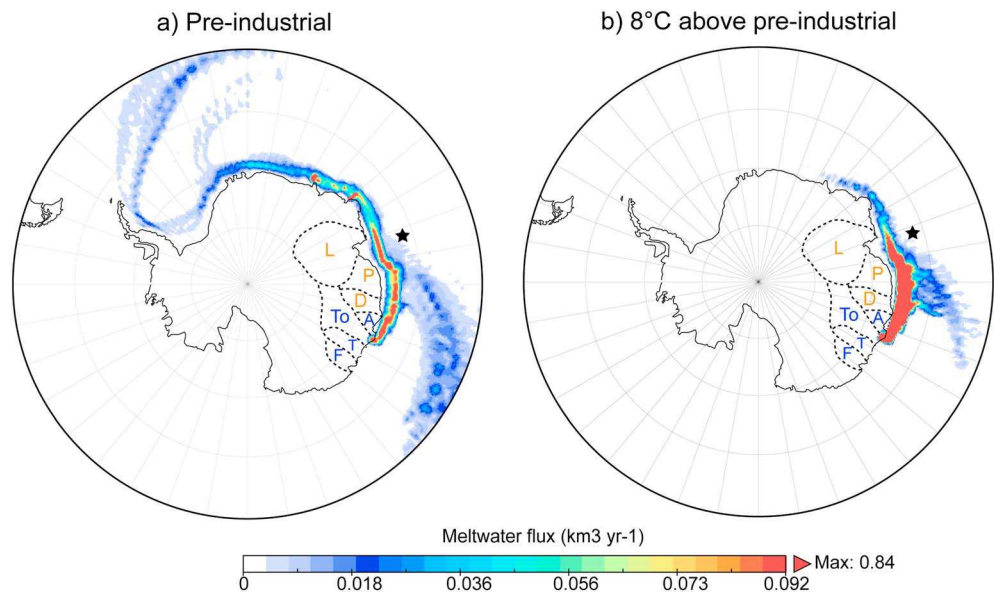


Figure 6. Iceberg meltwater input into the Southern Ocean in different SST scenarios from melting icebergs sourced from the Totten Glacier. The iceberg melt fraction in each grid cell was multiplied by the modern calving flux of the Totten (28 Gt yr^{-1}) [from *Rignot et al.*, 2013]. (a) Meltwater input in preindustrial control. (b) Meltwater input at 8°C above preindustrial. Maps also show location and catchment of the seven glacier systems used in our model, colored according to their location in the Prydz Bay sector (orange) or the Wilkes Land sector (blue). L: Lambert, P: Philippi, D: Denman, A: Adams, To: Totten, T: Thompson, and F: Frost Glaciers.

far-traveled Wilkes Land IRD in late Pliocene sediments suggests a similar increase in iceberg production in Wilkes Land and hints that other processes, such as SST, may have also played a role.

The observed increase in the relative abundance of Wilkes Land IRD in three of the eight IRD layers around $\sim 4.6 \text{ Ma}$ is accompanied by an overall increase in linear sedimentation rates, but IRD MAR show no significant increase over this interval. In addition, increased sedimentation rates and increased delivery of Wilkes Land IRD around $\sim 4.6 \text{ Ma}$ at Site 1165 correspond with increased biogenic opal content [*Passchier*, 2011] and warm SSTs as inferred from silicoflagellate assemblages [*Whitehead and Bohaty*, 2003; *Escutia et al.*, 2009]. These warm conditions were contemporaneous with evidence for ice sheet retreat both in the Prydz Bay area (see *Whitehead et al.* [2006] for a review), the Ross Sea [*Naish et al.*, 2009], and the Wilkes Subglacial Basin [*Cook et al.*, 2013]; hence, a scenario of ice sheet expansion onto the continental shelf is incompatible with the observed increased supply of Wilkes Land IRD during this interval (see section 8 for further discussion).

Iceberg detritus loading and iceberg production rates play an important role on IRD deposition on glacial-interglacial timescales [*Passchier*, 2011; *Patterson et al.*, 2011], with ice retreat during warmer climate conditions probably producing more detritus-laden icebergs than cooler, more stable, and “colder-based” advanced ice sheet margins [*Williams et al.*, 2010]. Retreat of the EAIS along the low-lying Wilkes Land margin in the vicinity of the Aurora Subglacial Basin seems feasible during warmer-than-present early Pliocene temperatures [*Young et al.*, 2011], contemporaneous with numerous interglacial retreat events in the neighboring Wilkes Subglacial Basin [*Cook et al.*, 2013]. While increased supply of Wilkes Land IRD at $\sim 4.6 \text{ Ma}$ is compatible with such a scenario (see section 8), lower abundances of Wilkes Land-derived IRD deposited at Site 1165 during the rest of the early Pliocene are unexpected.

7.1. Modeling of Iceberg Trajectories and Melting Patterns

In order to investigate the higher average relative abundance of far-traveled Wilkes Land IRD between 3.27 and 2.65 Ma during the relatively cooler middle to late Pliocene, in comparison to the relatively warmer early Pliocene, we consider the effect of changing SSTs on iceberg melting patterns using a coupled ocean-atmosphere general circulation model, HadCM3 [*Gordon et al.*, 2000], within a thermodynamic iceberg model [*Bigg et al.*, 1997; *Gladstone et al.*, 2001]. Seven distinct drainage basins were simulated, three located in the Prydz Bay area with icebergs seeded at the calving fronts of the Lambert, Philippi and Denman Glaciers, and

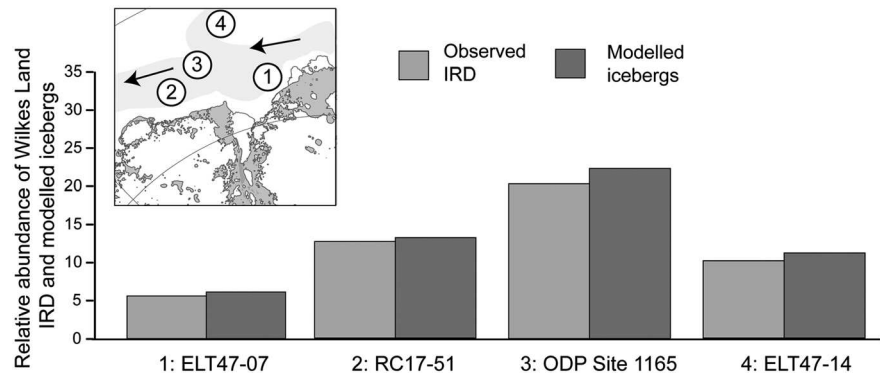


Figure 7. Histogram illustrating the data-model comparison for the relative abundance of Wilkes Land hornblende grains (light grey boxes; based on geochemical provenance data) and Wilkes Land iceberg melt (dark grey boxes; based on model outputs) at four sites located in the Prydz Bay region during the Holocene. Observed IRD provenance is inferred from $^{40}\text{Ar}/^{39}\text{Ar}$ age distributions of hornblende grains [Brachfeld et al., 2007; Roy et al., 2007; this study], with Wilkes Land sourced grains aged between 1000 and 1350 Ma. This comparison illustrates the excellent agreement between the observed amount of Wilkes Land IRD relative to Prydz Bay IRD during the Holocene and the modeled preindustrial amount of Wilkes Land-derived iceberg melt relative to Prydz Bay-derived iceberg melt.

four in Wilkes Land from the Adams, Totten, Thompson and Frost Glaciers (Figure 6). For each EAIS outlet glacier of interest the model was seeded with 1200 icebergs of different sizes (ranging from $40 \times 40 \times 60\text{m}$ to $250 \times 1467 \times 2200\text{m}$), in agreement with observed iceberg dimensions [Tchernia and Jeannin, 1980; Gladstone et al., 2001; Jacka and Giles, 2007; Stuart and Long, 2011]. One hundred icebergs were released in each month of a 12 month period from each drainage basin, with seasonally changing wind fields and surface currents taken from a preindustrial global climate model scenario (HadCM3). This modeling strategy is similar to previous simulations that reproduced observational data [Gladstone et al., 2001] (Antarctic Iceberg Tracking Database [1978–2012]; available at <http://www.scp.byu.edu/data/iceberg/database1.html>), with most icebergs traveling in an anticlockwise direction upon entrainment into the westward flowing coastal current (Figure 6a). A small number of Wilkes Land icebergs are diverted northward in the vicinity of the Kerguelen Plateau, likely due to its topographic influence on ocean currents, in agreement with modern observations [Tchernia and Jeannin, 1980] and previous modeling studies [Gladstone et al., 2001].

Evaluation of the suitability of our modeling framework was achieved by comparison of predicted iceberg melting patterns under preindustrial climate conditions with IRD provenance patterns of Holocene core-top sediments in the Prydz Bay area [Brachfeld et al., 2007; Roy et al., 2007; this study] (Figure 7). Importantly, as our model produces melting rates of icebergs and not IRD deposition patterns, any comparison to IRD depositional records assumes that melting rates of icebergs are proportional to melt out of IRD from icebergs produced from the same region. To permit for comparison of modeled iceberg melting patterns and IRD records, we assumed that the Lambert, Philippi, and Denman drainage basins represent 100% of the Prydz Bay-derived IRD signal, and the Adams, Totten, Thompson, and Frost basins represent 100% of Wilkes Land IRD signal. Despite these assumptions, this comparison exercise reveals excellent agreement between the observed relative abundance of Wilkes Land-derived hornblende grains in core-top sediments and the predicted iceberg melt rates over the sites that were sourced from Wilkes Land in preindustrial conditions (Figure 7).

Sensitivity tests were run for a range of SST scenarios between 1° and 8°C warmer than preindustrial levels (Figures 6 and 8). Results suggest that temperatures above 2°C drive a decrease in the amount of Wilkes Land icebergs melting at Site 1165 relative to Prydz Bay-supplied icebergs and reveal increasingly shorter iceberg tracks in increasingly warmer waters (Figures 6b and 8). These general trends are in agreement with observed late Pliocene IRD provenance patterns. For example, the doubling of Wilkes Land IRD after $\sim 3.27\text{Ma}$ (Figures 2 and 5) appears to closely follow declining regional SST records [Bohaty and Harwood, 1998; McKay et al., 2012] (Figure 5), suggesting decreased iceberg melt in the vicinity of Site 1165 from the nearby Prydz Bay glaciers and increasing iceberg melt sourced from the glaciers of Wilkes Land. We note that increased production of detritus-laden icebergs supplied from both the Prydz Bay and Wilkes Land sectors would be required to produce the tenfold increase in IRD MAR during this time. However, modeling results show that warm SSTs, such as those characteristic of the early Pliocene [Whitehead and Bohaty, 2003; Escutia et al., 2009; McKay et al., 2012], reduce

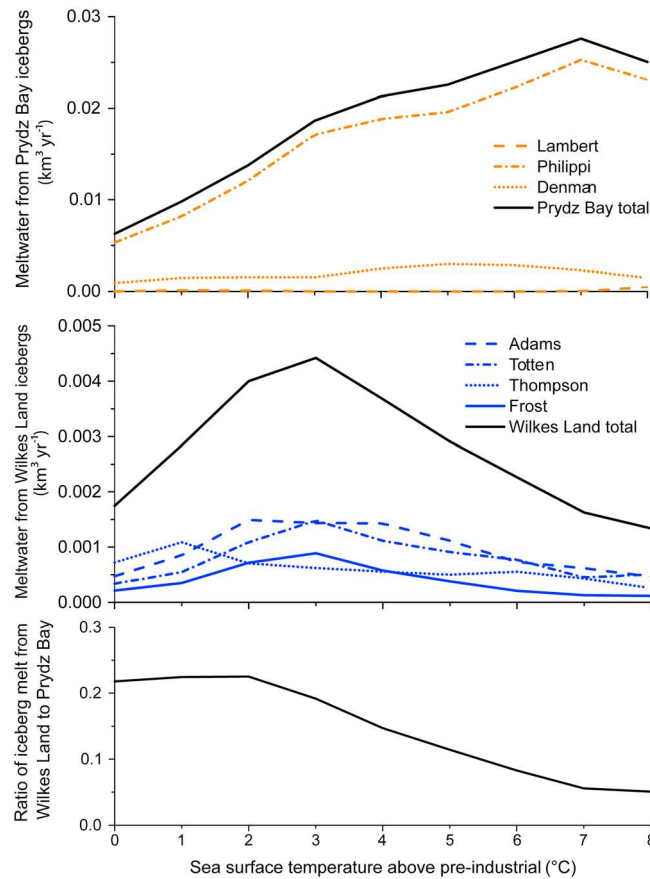


Figure 8. (top) Iceberg meltwater produced from Prydz Bay glaciers (in orange) and (middle) Wilkes Land glaciers (in blue), shown as a (bottom) ratio of Wilkes Land iceberg melt relative to Prydz Bay iceberg melt that melt over Site 1165 in different SST scenarios. Dashed lines represent the abundance of icebergs to melt from each modeled glacier, and solid lines represent the combined abundance of icebergs from each sector. The model results show an overall decline in Wilkes Land-sourced iceberg meltwater with increasing temperature.

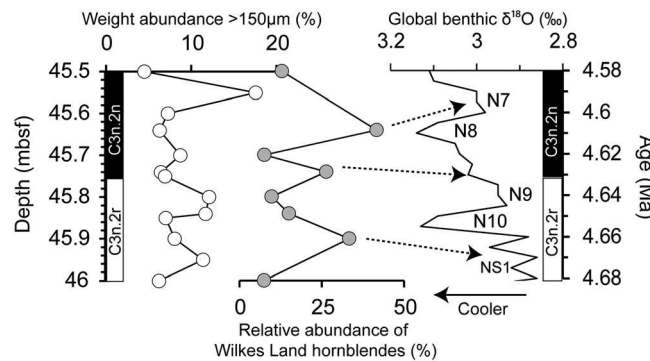


Figure 9. High-resolution section of Site 1165 between 46.00 and 45.50 m bsf. From left to right: (i) relative abundance of grain fractions >150 μm (this study); (ii) relative abundance of Wilkes Land hornblendes (this study); and (iii) global benthic oxygen isotope stack [Lisiecki and Raymo, 2005]. The boundary of the Nunivak subchron reversal at 4.631 Ma is based on the paleomagnetic and benthic $\delta^{18}\text{O}$ records of ODP Site 846 [Lisiecki and Raymo, 2005; from Shackleton et al., 1995].

the amount of Wilkes Land icebergs reaching Site 1165 by around 30% relative to the present day (assuming early Pliocene SSTs of 4°C warmer than preindustrial levels) (Figures 5 and 9). Thus, the increased relative abundances of Wilkes Land IRD at around 4.6 Ma require increased output of debris-rich icebergs from Wilkes Land, both to overcome the effect of faster melting and to increase levels of IRD at Site 1165 relative to locally derived IRD from Prydz Bay. We relate this increase in Wilkes Land IRD to instability in the Aurora Subglacial Basin (see section 8).

In addition to changing SSTs and iceberg production rates (see section 8 for further discussion), changes in iceberg transport in the coastal current could also have played a role on Southern Ocean IRD distribution during the Pliocene. For example, it is not known to what extent the strength of katabatic wind fields could be maintained during significant EAIS volume loss, even though model simulations suggest continued existence of katabatic winds even under reduced ice extent scenarios [DeConto et al., 2007]. If the coastal current was halted or reversed during the Pliocene, icebergs sourced from regions to the west of Prydz Bay could feasibly have reached our study site. However, bedrock terranes in western Enderby Land to the west of Prydz Bay and Mac.Robertson Land (Figure 1) are characterized by Archean (>2450 Ma; U-Pb zircon [Black and James, 1983; Harley and Black, 1997; Kelly and Harley, 2005] and Proterozoic (990–900, 1030–1100 Ma; U-Pb zircon) [Jacobs et al., 1998, 2003; Fitzsimons, 2000a, 2000b]) thermochronological ages that show only a small overlap with the Proterozoic $^{40}\text{Ar}/^{39}\text{Ar}$ hornblende ages observed in Site 1165 sediments (i.e., 1050 to 1315 Ma but centered around 1120 to 1175 Ma). Hence, we exclude a Pliocene supply of Proterozoic hornblende grains from sources to the west to Site 1165, and our data show that surface currents and iceberg transport pathways followed similar routes during the Pliocene and today.

While the direction of the coastal current was unchanged during the Pliocene, it is possible that strengthening wind fields would increase the speed of the coastal current and hence result in increased delivery of icebergs sourced from the east during times of ice sheet expansion, such as during the late Pliocene. While our data-model comparison reveals that SST-driven iceberg melting could have played a significant role in the delivery of far-traveled IRD to Site 1165 during the Pliocene, potentially reduced wind strengths and slower ocean current speeds combined with warmer SST's during intervals of enhanced regional warming such as within the early Pliocene would be expected to result in decreased supply of Wilkes Land IRD to Site 1165.

8. Evidence for Early Pliocene Destabilization in the Aurora Subglacial Basin

Sea surface temperature estimates from early Pliocene silicoflagellate assemblages at Site 1165 [Whitehead and Bohaty, 2003; Escutia et al., 2009] suggest that some interglacials were more than 6°C warmer than present (Figure 5). Our iceberg modeling implies that such temperatures are sufficient to reduce the Wilkes Land iceberg supply at Site 1165 by 50% relative to cooler temperatures of ~3°C, with a maximum of 10% relative abundance of Wilkes Land icebergs at 6°C (Figure 8). However, significantly higher relative abundances of Wilkes Land IRD are actually observed around 4.6 Ma (up to 42%) (Figure 5). Importantly, available high-resolution IRD MAR records [Passchier, 2011; Patterson et al., 2011] show that orbital-scale fluctuations in ice volume also exert a major control on Pliocene IRD flux to the Southern Ocean during the Pliocene. Samples analyzed around 4.6 Ma reveal a high degree of variability in the relative abundance of Wilkes Land IRD over three to four glacial-interglacial cycles (Figure 9). Although the resolution of the age model is not sufficient to assign precise ages to most of the IRD layers, one sample is located 1 cm upcore from the middle of the Nunivak subchron reversal (C3n.2r), which most likely occurred during the marine isotope stage N9 interglacial ~4.631 Ma [Lisiecki and Raymo, 2005; Gradstein et al., 2012]. Importantly, this sample (45.74 m bsf) is characterized by higher amounts of Wilkes Land IRD.

Results of our iceberg modeling combined with regional SST estimates for the early Pliocene indicate that a scenario of increased Wilkes Land IRD during an early Pliocene interglacial would require significantly greater production of icebergs from the Wilkes Land margin in order to survive melting while traveling over 1500 km to reach Site 1165. Based on the modeled increased melt with increased SSTs and the measured increases in IRD delivery, such events would require a fivefold to ninefold increase in iceberg production rates from the Wilkes Land margin relative to baseline values during an interglacial. These higher values are comparable to estimates of increased iceberg production rates associated with the deposition of Heinrich layers in the Hudson Strait region in the North Atlantic (ninefold to eighteenfold increase from baseline levels) [McManus et al., 1998; Roberts et al., 2014], which were associated with large-scale surging and collapse of ice streams within the Laurentide Ice Sheet. The large increase in IRD MAR at Site 1165 between 3.3 and 3.0 Ma does also require a dramatic increase in the production of debris-rich icebergs from both the Wilkes Land and Prydz Bay sectors. However, the overall doubling of the proportion of Wilkes Land IRD relative to Prydz Bay IRD during this interval can be best explained by declining SSTs allowing more of the Wilkes Land icebergs to reach Site 1165.

A scenario of large-scale EAIS destabilization could explain increases in Wilkes Land IRD deposition during early Pliocene interglacials at Site 1165; whereby, retreat of the ice sheet in the Aurora Subglacial Basin took place during warmer-than-present conditions, as originally suggested by Williams et al. [2010]. This scenario is compatible with contemporaneous retreat of the EAIS in the Wilkes Subglacial Basin [Cook et al., 2013], implying that an even higher resolved IRD provenance study at Site 1165 could provide further evidence of enhanced iceberg production supplied from a retreating ice sheet margin in the Aurora Subglacial Basin during Pliocene interglacials. In addition to contributing to eustatic sea level rise, such large iceberg production events could have had significant implications for meltwater input [Lichey and Hellmer, 2001; Death et al., 2006], latent heat transfer [e.g., Jongma et al., 2009], and biological productivity [Raiswell et al., 2006; Smith et al., 2007; Lin et al., 2011] in the Southern Ocean during the Pliocene.

9. Conclusions

Here we present a Pliocene IRD provenance record based on the $^{40}\text{Ar}/^{39}\text{Ar}$ ages of ice-rafted hornblende grains from ODP Site 1165, near Prydz Bay, along with the results of modeled sensitivity tests of iceberg trajectories and their spatial melting patterns under different SSTs. Our IRD provenance record and iceberg

modeling reveal that declining regional SSTs during the late Pliocene permitted for an increase in the deposition of remotely sourced IRD at Site 1165. Superimposed upon low average amounts of Wilkes Land IRD during the early Pliocene, related to warm SSTs, is a variable IRD provenance signal that hints at massive iceberg production events, possibly associated with large-scale destabilization in the Aurora Subglacial Basin during interglacial periods. These new findings suggest that SST reconstructions are crucial for the interpretation of past IRD distribution and provenance records when inferring past ice sheet variability from IRD deposited in distal locations.

Acknowledgments

Data presented here are freely available upon request. The authors would like to thank Sandra Passchier for providing data and discussion, Ian Bailey and Nathalie Fagel for constructive reviews, and Heiko Pälke for speedy editorial handling. Grant Biggs and William Roberts are acknowledged for providing access to the iceberg model and climate input routines. C.P. Cook thanks the Grantham Institute for Climate Change for a PhD scholarship, K. Kreissig and B. Coles for lab assistance, and the Ocean Drilling Program for providing materials. D.J. Hill acknowledges the Leverhulme Trust for the award of an Early Career Fellowship and the National Centre for Atmospheric Science and the British Geological Survey for financial support. T.v.d. Flierdt acknowledges NERC UK IODP grant (NE/H014144/1) awarded to T.v.d. F. and A. Haywood (Leeds), a Marie Curie Reintegration grant (IRG 230828), and a Royal Society international exchange grant (IE110878) also awarded to S.R. Hemming. T.v.d. Flierdt, S.R. Hemming, and T. Williams also acknowledge NSF grant (ANT 0944489). C. Escutia acknowledges the Spanish Ministry of Science (Innovation grant CTM2011-24079). A.M.D. acknowledges the Natural Environment Research Council (NERC) for the provision of a doctoral training grant and also funding from the European Research Council under the European Union's Seventh Framework Programme (FP7/2007–2013)/ERC grant agreement n° 278636.

References

- Bailey, I., G. M. Hole, G. L. Foster, P. A. Wilson, C. D. Storey, C. N. Trueman, and M. E. Raymo (2013), An alternative suggestion for the Pliocene onset of major Northern Hemisphere glaciation based on the geochemical provenance of North Atlantic Ocean ice-rafted debris, *Quat. Sci. Rev.*, *75*, 181–194.
- Bailey, I., G. L. Foster, P. A. Wilson, L. Jovane, C. D. Storey, C. N. Trueman, and J. Becker (2012), The flux and provenance of ice-rafted debris in the earliest Pleistocene subpolar North Atlantic Ocean comparable to that of the Last Glacial maximum, *Earth Planet. Sci. Lett.*, *341–344*, 222–233, doi:10.1016/j.epsl.2012.05.034.
- Bamber, J. L., R. L. Layberry, and S. P. Gogineni (2001), A new ice thickness and bed data set for the Greenland ice sheet: 1. Measurement, data reduction and errors, *J. Geophys. Res.*, *106*, 33,773–33,780, doi:10.1029/2001JD900054.
- Bart, P. J., and M. Iwai (2012), The overdeepening hypothesis: How erosional modification of the marine-scape during the early Pliocene altered glacial dynamics on the Antarctic Peninsula's Pacific margin, *Palaeogeogr. Palaeoclimatol. Palaeoecol.*, *35–36*, 42–51, doi:10.1016/j.palaeo.2011.06.010.
- Bigg, G. R., et al. (1997), Modelling the dynamics and thermodynamics of icebergs, *Cold Reg. Sci. Technol.*, *26*(2), 113–135.
- Black, L. P., and P. R. James (1983), Geological history of the Archaean Napier complex of Enderby Land, in *Antarctic Earth Science*, edited by R. L. Oliver, P. R. James, and J. B. Jago, pp. 11–15, Australian Academy of Science, Canberra.
- Black, L. P., P. D. Kinny, J. W. Sheraton, and C. P. Delor (1991), Rapid production and evolution of Late Archaean felsic crust in the Vestfold Block of East Antarctica, *Precambrian Res.*, *50*(3–4), 283–310.
- Boger, S. D., C. J. Carson, C. M. Fanning, J. M. Hergt, C. J. L. Wilson, and J. D. Woodhead (2002), Pan-African intraplate deformation in the northern Prince Charles Mountains, East Antarctica, *Earth Planet. Sci. Lett.*, *195*(3–4), 195–210.
- Boger, S. D. (2011), Antarctica—Before and after Gondwana, *Gondwana Res.*, *19*(2), 335–371, doi:10.1016/j.gr.2010.09.003.
- Bohaty, S. M., and D. M. Harwood (1998), Southern Ocean Pliocene paleotemperature variation from high-resolution silicoflagellate biostratigraphy, *Mar. Micropaleontol.*, *33*(3–4), 241–272.
- Brachfeld, S. A., et al. (2007), Integrated provenance characteristics of glacial-marine sediment from East and West Antarctica, Antarctica: A Keystone in a Changing World, in *Proceedings of the 10th International Symposium on Antarctic Earth Sciences*, Santa Barbara, Calif.
- Carson, C. J., S. D. Boger, C. M. Fanning, C. J. L. Wilson, and D. E. Thost (2000), SHRIMP U-Pb geochronology from Mount Kirkby, northern Prince Charles Mountains, East Antarctica, *Antarct. Sci.*, *12*(4), 429–442.
- Clark, D. J., B. J. Hensen, and P. D. Kinny (2000), Geochronological constraints for a two-stage history of the Albany-Fraser Orogen, Western Australia, *Precambrian Res.*, *102*(3–4), 155–183.
- Clark, N. A., M. Williams, D. J. Hill, P. G. Quilty, J. L. Smellie, J. Zalasiewicz, M. J. Leng, and M. A. Ellis (2013), Fossil proxies of near-shore sea surface temperatures and seasonality from the late Neogene Antarctic shelf, *Naturwissenschaften*, *100*, 699–722.
- Clarke, C. L., S. S. Sun, and R. W. White (1995), Grenville age belts and adjacent older terranes in Australia and Antarctica, *J. Aust. Geol. Geophys.*, *16*, 441–450.
- Cook, C. P., et al. (2013), Dynamic behaviour of the East Antarctic Ice Sheet during Pliocene warmth, *Nat. Geosci.*, *6*, 765–769, doi:10.1038/ngeo1889.
- Cook, C. P. (2013), Insights into the behaviour of the Pliocene East Antarctic Ice Sheet from provenance studies of marine sediments using radiogenic isotopes, PhD thesis, Imperial College London.
- Cortese, G., and R. Gersonde (2008), Plio/Pleistocene changes in the main biogenic silica carrier in the Southern Ocean, Atlantic Sector, *Mar. Geol.*, *252*, 100–110.
- Corvino, A. F., S. D. Boger, F. Henjes-Kunst, C. J. L. Wilson, and I. C. W. Fitzsimons (2008), Superimposed tectonic events at 2450 Ma, 2100 Ma, 900 Ma and 500 Ma in the North Mawson Escarpment, Antarctic Prince Charles Mountains, *Precambrian Res.*, *167*(3–4), 281–302.
- Corvino, A. F., C. J. L. Wilson, and S. D. Boger (2011), The structural and tectonic evolution of a Rodinian continental fragment in the Mawson Escarpment, Prince Charles Mountains, Antarctica, *Precambrian Res.*, *184*(1–4), 70–92.
- Dalrymple, G. E., et al. (1981), Irradiation of samples for $^{40}\text{Ar}/^{39}\text{Ar}$ dating using the Geological Survey TRIGA reactor, *U.S. Geol. Surv. Prof. Pap.*, *1176*.
- Death, R., M. J. Siegert, G. R. Bigg, and M. R. Wadley (2006), Modelling iceberg trajectories, sedimentation rates and meltwater input to the ocean from the Eurasian Ice Sheet at the Last Glacial Maximum, *Palaeogeogr. Palaeoclimatol. Palaeoecol.*, *236*, 135–150.
- DeConto, R., D. Pollard, and D. Harwood (2007), Sea ice feedback and Cenozoic evolution of Antarctic climate and ice sheets, *Paleoceanography*, *22*, PA3214, doi:10.1029/2006PA001350.
- Dolan, A. M., A. M. Haywood, D. J. Hill, H. J. Dowsett, S. J. Hunter, D. J. Lunt, and S. J. Pickering (2011), Sensitivity of Pliocene ice sheets to orbital forcing, *Palaeogeogr. Palaeoclimatol. Palaeoecol.*, *309*, 98–110, doi:10.1016/j.palaeo.2011.03.030.
- Downing, G. E., and S. R. Hemming (2012), Late glacial and deglacial history of ice rafting in the Labrador Sea: A perspective from radiogenic isotopes in marine sediments, *Geol. Soc. Am. Spec. Pap.*, *487*, 113–124.
- Escutia, C., et al. (2009), Circum-Antarctic warming events between 4 and 3.5 Ma recorded in marine sediments from the Prydz Bay (ODP Leg 188) and the Antarctic Peninsula (ODP Leg 178) margins, *Global Planet. Change*, *69*(3), 170–184.
- Fitzsimons, I. C. W. (2000a), Grenville-age basement provinces in East Antarctica: Evidence for three separate collisional orogens, *Geology*, *28*(10), 879–882.
- Fitzsimons, I. C. W. (2000b), A review of tectonic events in the East Antarctic Shield and their implications for Gondwana and earlier supercontinents, *J. Afr. Earth. Sci.*, *31*(1), 3–23.
- Florindo, F., S. M. Bohaty, P. S. Erwin, C. Richter, A. P. Roberts, P. A. Whalen, and J. M. Whitehead (2003), Magnetobiostratigraphic chronology and palaeoenvironmental history of Cenozoic sequences from ODP sites 1165 and 1166, Prydz Bay, Antarctica, *Palaeogeogr. Palaeoclimatol. Palaeoecol.*, *198*(1–2), 69–100.
- Fretwell, P., et al. (2013), Bedmap2: Improved ice bed, surface and thickness datasets for Antarctica, *Cryosphere*, *7*, 375–393.

- Gladstone, R. M., G. R. Bigg, and K. W. Nicholls (2001), Iceberg trajectory modelling and meltwater injection in the Southern Ocean, *J. Geophys. Res.*, *106*(19), 903–19, doi:10.1029/2000JC000347.
- Gordon, C., C. Cooper, C. A. Senior, H. Banks, J. M. Gregory, T. C. Johns, J. F. B. Mitchell, and R. A. Wood (2000), The simulation of SST, sea ice extents and ocean heat transports in a version of the Hadley Centre coupled model without flux adjustments, *Clim. Dyn.*, *16*(2–3), 147–168.
- Gradstein, F., J. Ogg, M. Schmitz, and G. Ogg (2012), *The Geological Time Scale*, Elsevier.
- Grutznier, J., et al. (2003), Data report: Multisensor core logging data, coarse fraction grain-size analyses, and biogenic silica content of upper Miocene-lower Pliocene sediments, ODP Site 1165, in *Proceedings of the Ocean Drilling Program, Scientific Results*, vol. 188, edited by A. K. Cooper, P. E. O'Brien, and C. Richter, pp. 1–16, Ocean Drilling Program, College Station, Tex.
- Halpin, J. A., G. L. Clarke, R. W. White, and D. E. Kelsey (2007), Contrasting P-T-t paths for Neoproterozoic metamorphism in MacRobertson and Kemp Lands, East Antarctica, *J. Metamorph. Geol.*, *25*(6), 683–701.
- Harley, S. L., and L. P. Black (1997), A revised Archean chronology for the Napier Complex, Enderby Land, from SHRIMP ion-microprobe studies, *Antarct. Sci.*, *9*, 74–91.
- Hayes, D. E., et al. (1975), Site 274, initial report: Deep Sea Drilling Program, Expedition 28, 369–433.
- Hemming, S. R. (2004), Heinrich events: Massive late Pleistocene detritus layers of the North Atlantic, and their global climate imprint, *Rev. Geophys.*, *42*, RG1005, doi:10.1029/2003RG000128.
- Hill, D. J., et al. (2007), Characterising ice sheets during the Pliocene: Evidence from data and models, in *Deep Time Perspectives on Climate Change*, edited by M. Williams et al., pp. 517–538, The Micropalaeontological Society/ The Geological Society of London, London.
- Jacka, T. H., and A. B. Giles (2007), Antarctic iceberg distribution and dissolution for correlations from ship-based observations, *J. Glaciol.*, *53*(182), 341–356.
- Jacobs, J., et al. (1998), Continuation of the Mozambique Belt into East Antarctica: Grenville-age metamorphism and polyphase Pan-African high-grade events in central Dronning Maud Land, *J. Geol.*, *106*(4), 385–406.
- Jacobs, J., C. M. Fanning, and W. Bauer (2003), Timing of Grenville-age vs. Pan-African medium- to high grade metamorphism in western Dronning Maud Land (East Antarctica) and significance for correlations in Rodinia and Gondwana, *Precambrian Res.*, *125*(1–2), 1–20.
- Jongma, J. I., et al. (2009), The effect of dynamic-thermodynamic iceberg on the Southern Ocean climate in a three-dimensional model, *Ocean Modell.*, *26*, 104–113.
- Kelly, N. M., and S. L. Harley (2005), An integrated microtextural and chemical approach to zircon geochronology: Refining the Archaean history of the Napier Complex, East Antarctica, *Contrib. Mineral. Petrol.*, *149*(1), 57–84.
- Lichey, C., and H. H. Hellmer (2001), Modeling giant-iceberg drift under the influence of sea ice in the Weddell Sea, Antarctica, *J. Glaciol.*, *47*(158), 452–460.
- Lin, H., S. Rauschenberg, C. R. Hexel, T. J. Shaw, and B. S. Twining (2011), Free-drifting icebergs as sources of iron to the Weddell Sea, *Deep Sea Res. Part II*, *58*(11–12), 1392–1406.
- Lisiecki, L. E., and M. E. Raymo (2005), A Pliocene-Pleistocene stack of 57 globally distributed benthic $\delta^{18}O$ records, *Paleoceanography*, *20*, PA1003, doi:10.1029/2004PA001071.
- Liu, X. C., B.-m. Jahn, Y. Zhao, M. Li, H. Li, and X. Liu (2006), Late Pan-African granulites from the Grove Mountains, East Antarctica: Age, origin and tectonic implications, *Precambrian Res.*, *145*(1–2), 131–154.
- Liu, X. C., B.-M. Jahn, Y. Zhao, G. Zhao, and X. Liu (2007), Geochemistry and geochronology of high-grade rocks from the Grove Mountains, East Antarctica: Evidence for an Early Neoproterozoic basement metamorphosed during a single Late Neoproterozoic/Cambrian tectonic cycle, *Precambrian Res.*, *158*(1–2), 93–118.
- Ludwig, K. R. (2003), *Isoplot—A Geochronological Toolkit for Microsoft Excel*, Berkeley Geochronology Center, Berkeley, Calif.
- McCollum, D. W. (1975), Diatom stratigraphy of the Southern Ocean, in *Init. Repts. DSDP*, vol. 28, edited by D. E. Hayes et al., pp. 515–571, U.S. Govt. Printing Office, Washington.
- McDougall, I., and T. M. Harrison (1999), *Geochronology and Thermochronology by the $^{40}Ar/^{39}Ar$ Method*, Oxford Univ. Press, Oxford.
- McKay, R., et al. (2012), Antarctic and Southern Ocean influences on Late Pliocene global cooling, *Proc. Natl. Acad. Sci. U.S.A.*, *109*(17), 6423–6428.
- McManus, J. F., et al. (1998), Radiometrically determined sedimentary fluxes in the sub-polar North Atlantic during the last 140,000 years, *Earth Planet. Sci. Lett.*, *155*(1–2), 29–43.
- Naish, T., et al. (2009), Obliquity-paced Pliocene West Antarctic ice sheet oscillations, *Nature*, *458*(7236), 322–328, doi:10.1038/nature07867.
- O'Brien, P. E., I. Goodwin, C.-F. Forsberg, A. K. Cooper, and J. Whitehead (2007), Late Neogene ice drainage changes in Prydz Bay, East Antarctica and the interaction of Antarctic ice sheet evolution and climate, *Palaeogeogr. Palaeoclimatol. Palaeoecol.*, *245*(3–4), 390–410.
- Passchier, S. (2011), Linkages between East Antarctic Ice Sheet extent and Southern Ocean temperatures based on a Pliocene high-resolution record of ice-rafted debris off Prydz Bay, East Antarctica, *Paleoceanography*, *26*, PA4204, doi:10.1029/2010PA002061.
- Patterson, M. O., et al. (2011), Pliocene sedimentary processes off the East Antarctic Ice Sheet margin of Wilkes Land, Antarctica, Abstract PP33B-1925 presented at 2010 Fall Meeting, AGU, San Francisco, Calif.
- Peck, V. L., I. R. Hall, R. Zahn, F. Grousset, S. R. Hemming, and J. D. Scourse (2007), The relationship of Heinrich events and their European precursors over the past 60 ka BP: A multi-proxy ice-rafted debris provenance study in the North East Atlantic, *Quat. Sci. Rev.*, *26*, 862–875.
- Phillips, G., C. J. L. Wilson, D. Phillips, and S. K. Szczepanski (2007), Thermochronological ($^{40}Ar/^{39}Ar$) evidence of Early Palaeozoic basin inversion within the southern Prince Charles Mountains, East Antarctica: Implications for East Gondwana, *J. Geol. Soc.*, *164*, 771–784.
- Pierce, E. L., T. Williams, T. van de Fliert, S. R. Hemming, S. L. Goldstein, and S. A. Brachfeld (2011), Characterizing the sediment provenance of East Antarctica's weak underbelly: The Aurora and Wilkes sub-glacial basins, *Paleoceanography*, *26*, PA4217, doi:10.1029/2011PA002127.
- Piper, D. J. W., and C. D. Brisco (1975), Deep water continental margin sedimentation, Leg 28 Antarctica, in *Initial Reports of the DSDP*, vol. 28, edited by D. E. Hayes et al., pp. 727–755, U. S. Government Printing Office, Washington, D. C.
- Post, N. J., B. J. Hensen, and P. D. Kinny (1996), Two metamorphic episodes during a 1340–1180 Ma convergent tectonic event in the Windmill Islands, East Antarctica, in *The Antarctic Region; Geological Evolution and Processes*, in *Proceedings of the VII International Symposium of Antarctic Earth Sciences*, edited by C. A. Ricci, pp. 157–161, Terra Antarctica, Siena.
- Raiswell, R., M. Tranter, L. G. Benning, M. Siegert, R. De'ath, P. Huybrechts, and T. Payne (2006), Contributions from glacially derived sediment to the global iron (oxyhydr)oxide cycle: Implications for iron delivery to the oceans, *Geochim. Cosmochim. Acta*, *70*(11), 2765–2780.
- Rebesco, M., A. Camerlenghi, R. Geletti, and M. Canals (2006), Margin architecture reveals the transition to the modern Antarctic ice sheet ca. 3 Ma, *Geology*, *34*(4), 301–304.
- Rignot, E., S. Jacobs, J. Mougnot, and B. Scheuchl (2013), Ice-shelf melting around Antarctica, *Science*, *341*, 266–270, doi:10.1126/science.1235798.
- Roberts, W. G., P. J. Valdes, and A. J. Payne (2014), A new constraint on the size of Heinrich Events from an iceberg/sediment model, *Earth Planet. Sci. Lett.*, *386*, 1–9.
- Roy, M., T. van de Fliert, S. R. Hemming, and S. L. Goldstein (2007), ($^{40}Ar/^{39}Ar$) ages of hornblende grains and bulk Sm/Nd isotopes of circum-Antarctic glacio-marine sediments: Implications for sediment provenance in the Southern Ocean, *Chem. Geol.*, *244*(3–4), 507–519.
- Samson, S. D., and E. C. Alexander (1987), Calibration of the interlaboratory $^{40}Ar/^{39}Ar$ dating standard, MMHB-1, *Chem. Geol.*, *66*(1–2), 27–34.

- Schoof, C. (2007), Marine ice-sheet dynamics. Part 1. The case of rapid sliding, *J. Fluid. Mech.*, *573*, 27–55.
- Shackleton, N. J., S. Crowhurst, T. Hagelberg, N. G. Pisias, and D. A. Schneider (1995), A new late Neogene time scale: Application to Leg 138 sites, in *Proc. ODP, Sci. Results*, vol. 138, edited by N. G. Pisias et al., pp. 73–101, Ocean Drilling Program, College Station, Tex., doi:10.2973/odp.proc.sr.138.106.1995
- Sheraton, J. W., L. P. Black, and A. G. Tindle (1992), Petrogenesis of plutonic rocks in a Proterozoic granulite-facies terrane—The Bunge Hills, East Antarctica, *Chem. Geol.*, *97*(3–4), 163–198.
- Sheraton, J. W., R. J. Tingey, L. P. Black, and R. L. Oliver (1993), Geology of the Bunge Hills area, Antarctica: Implications for Gondwana reconstructions, *Antarct. Sci.*, *5*, 85–102.
- Smith, K. L., Jr., B. H. Robison, J. J. Helly, R. S. Kaufmann, H. A. Ruhl, T. J. Shaw, B. S. Twining, and M. Vernet (2007), Free-drifting icebergs: Hot spots of chemical and biological enrichment in the Weddell Sea, *Science*, *317*, 478–482, doi:10.1126/science.1142834.
- Stuart, K. M., and D. G. Long (2011), Tracking large tabular icebergs using the SeaWinds Ku-band microwave scatterometer, *Deep Sea Res., Part II*, *58*, 1285–1300, doi:10.1016/j.dsr2.2010.11.004.
- Takigami, Y., M. Funaki, and K. Tokieda (1992), 40Ar/39Ar geochronological studies on some paleomagnetic samples of East Antarctica, in *Recent Progress in Antarctic Earth Science*, edited by Y. Yoshida et al., pp. 61–66, Terra Scientific Publishing Group, Tokyo.
- Tchernia, P., and P. F. Jeannin (1980), Observations on the Antarctic East Wind Drift using tabular icebergs tracked by satellite Nimbus 7 (1975–1977), *Deep Sea Res.*, *7*(6), 467–474.
- Thierens, M., et al. (2012), Ice-rafting from the British-Irish ice sheet since the earliest Pleistocene (2.6 million years ago): Implications for long-term mid-latitude ice-sheet growth in the North Atlantic regions, *Quat. Sci. Rev.*, *44*, 229–240, doi:10.1016/j.quascirev.2010.12.020.
- Tochilin, C. J., P. W. Reiners, S. N. Thomson, G. E. Gehrels, S. R. Hemming and E. L. Pierce (2012), Erosional history of the Prydz Bay sector of East Antarctica from detrital apatite and zircon geo- and thermochronology multidating, *Geochem. Geophys. Geosyst.*, *13*, Q11015, doi:10.1029/2012GC004364
- Tong, L., C. J. L. Wilson, and X. C. Liu (2002), A high-grade event of 1100 Ma preserved within the ~500 Ma mobile belt of Larsemann Hills, East Antarctica: Further evidence from 40Ar/39Ar dating, *Terra Antarct.*, *9*, 73–86.
- Volpi, V., M. Rebesco, and P. Diviacco (2009), New insights in the evolution of Antarctic glaciation from depth conversion of well-log calibrated seismic section of Prydz Bay, *Int. J. Earth Sci.*, *98*(8), 1991–2007.
- Warnke, D. A., et al. (2004), Data report: HiRISC (High-Resolution Integrated Stratigraphic Committee) Pliocene-Pleistocene interval, 0–50 m bsf, at ODP Leg 188 Site 1165, Prydz Bay, Antarctica, in *Proc. ODP, Sci. Results*, vol. 188, Ocean Drilling Program, College Station, Tex.
- Whitehead, J. M., and S. M. Bohaty (2003), Pliocene summer sea surface temperature reconstruction using silicoflagellates from Southern Ocean ODP Site 1165, *Paleoceanography*, *18*(3), 1075, doi:10.1029/2002PA000829
- Whitehead, J. M., P. G. Quilty, B. C. Mckelvey, and P. E. O'Brien (2006), A review of the Cenozoic stratigraphy and glacial history of the Lambert Graben-Prydz Bay region, East Antarctica, *Antarct. Sci.*, *18*(1), 83–99, doi:10.1017/S0954102006000083.
- Williams, T., T. van de Fliert, S. R. Hemming, E. Chung, M. Roy, and S. L. Goldstein (2010), Evidence for iceberg armadas from East Antarctica in the Southern Ocean during the late Miocene and early Pliocene, *Earth Planet. Sci. Lett.*, *290*(3–4), 351–361.
- Wilson, C. J. L., C. Quinn, L. Tong, and D. Phillips (2007), Early Paleozoic intracratonic shears and post-tectonic cooling in the Rauer Group, Prydz Bay, East Antarctica, constrained by 40Ar/39Ar thermochronology, *Antarct. Sci.*, *19*(3), 339–353.
- Young, D. A., et al. (2011), A dynamic early East Antarctic Ice Sheet suggested by ice-covered fjord landscapes, *Nature*, *474*(7349), 72–75, doi:10.1038/nature10114.
- Young, D. N., and L. P. Black (1991), U-Pb zircon dating of Proterozoic igneous charnockites from the Mawson coast, East Antarctica, *Antarct. Sci.*, *3*, 205–216.
- Young, D. N., J. X. Zhao, D. J. Ellis, and M. T. McCulloch (1997), Geochemical and Sr-Nd isotopic mapping of source provinces for the Mawson charnockites, east Antarctica: Implications for Proterozoic tectonics and Gondwana reconstruction, *Precambrian Res.*, *86*(1–2), 1–19.